- 1 Running head: Abrupt change in N₂O
- 2 An intense precipitation event causes a temperate forested drainage network
- 3 to shift from N₂O source to sink
- 4 K. S. Aho¹, J. H. Fair¹, J. D. Hosen^{1†}, E. D. Kyzivat^{1††}, L. Logozzo¹, L. C. Weber¹, B. Yoon^{1†††},
- 5 J. P. Zarnetske², P. A. Raymond¹
- 6 School of the Environment, Yale University, New Haven, CT, USA.
- ²Department of Earth and Environmental Sciences, Michigan State University, East Lansing, MI,
- 8 USA
- 9 † Department of Forestry and Natural Resources, Purdue University, West Lafayette, IN 47905
- 10 https://orcid.org/0000-0003-2559-0687
- 11 †† Department of Earth, Environmental & Planetary Sciences, Brown University, Providence, RI
- 12 02912; Institute at Brown for Environment and Society, Brown University, Providence, RI
- 13 02912
- 14 ††† Departments of Marine & Environmental Sciences, Chemistry & Chemical Biology, and Civil
- Land 15 & Environmental Engineering, Northeastern University, Boston, Massachusetts, USA
- 16 https://orcid.org/0000-0002-8959-3855
- 17 Corresponding author: Kelly Aho (kelly.aho@yale.edu) https://orcid.org/0000-0002-1992-6378
- 18 Keywords: Nitrous oxide, Streams, Rivers, Disturbance, Abrupt change

21 Abstract

Nitrous oxide (N2O) evasion from streams and rivers is a significant, yet highly
uncertain, flux in nitrogen cycle models. Most global estimates of lotic $N_2\mathrm{O}$ emission assume
that evasion rates are proportional to inorganic nitrogen inputs to a stream or river. However,
many field studies do not detect relationships between lotic $N_2\mathrm{O}$ evasion and dissolved nitrogen
concentration, highlighting the need for better understanding of process-based controls on this
flux. This study reports four-year time series of pN2O and N2O evasion from eight nested
streams and rivers and detects an abrupt change in N2O dynamics associated with an intense
rainstorm. This rainstorm, and the associated hydrologic flood event, pushed forested reaches
across the watershed from consistent N_2O sources to prolonged N_2O sinks on an annual basis.
We attribute this shift to disturbance of incomplete denitrification in the stream network and
surrounding watershed, although alternate hypotheses are also discussed. There was continued
availability of NO ₃ - for in-stream processing, eliminating the possibility that NO ₃ - availability
limited N_2O production, and post-storm N_2O -to-nitrate ratios were lower than pre-storm ratios
suggesting that the large storm affected in-situ nitrogen processing rates. The sustained period of
post-storm N_2O undersaturation resulted in net negative evasion for 2018 at fives of the eight
study sites, which mitigated emissions over the four-year study. This nonlinear response in $\ensuremath{N_2}\ensuremath{O}$
dynamics illustrates the potential importance of storm events to control lotic N_2O production and
emissions.

Significance Statement

Nitrous oxide (N ₂ O) is a potent greenhouse gas that contributes to global warming.
Nitrogen undergoes biogeochemical transformations in streams and rivers, which can result in
production and emission of N_2O . Most riverine N_2O emission models are based on nitrogen
loading and emission factors, or the proportion of nitrogen inputs converted to and released as
N ₂ O. These emission factors are highly uncertain, and field studies challenge their broad
applicability. In this study, we present four-year time series of N ₂ O dynamics in eight streams
and rivers. We find that a large rainstorm caused a decrease in N_2O concentration and emission
rates that was sustained for up to a year. The storm pushed forested streams and rivers from $N_2\mathrm{O}$
sources to N ₂ O sinks, despite the continued presence of inorganic nitrogen. This non-linear
response is attributed to disturbance of incomplete denitrification in the streambed and the
surrounding watershed and is relevant to aquatic nitrogen cycling and to $N_2\mathrm{O}$ budgets.

63 Introduction

Nitrous oxide (N_2O) evasion from streams and rivers is a significant, yet highly
uncertain, flux in the global nitrogen budget. The two most recent global emission estimates
from streams and rivers disagree by a factor of four: 291 Gg-N yr ⁻¹ (Yao et al. 2020) and 72.8
Gg-N yr ⁻¹ (Marzadri et al. 2021). Further, global riverine evasion estimates were much higher
~10-20 years ago due to changing modeling methodologies (e.g., 1260 Gg-N yr ⁻¹ in Kroeze et al
2005 and 680 Gg-N yr ⁻¹ in Beaulieu et al. 2011). Most estimates of N ₂ O emission from streams
and rivers are based on dissolved inorganic nitrogen (DIN) loading and emission factors (EFs),
or ratios that predict N ₂ O emission from nitrate (NO ₃ -) or total nitrogen (TN) loading (Seitzinger
and Kroeze 1998; Beaulieu et al. 2011; Hu et al. 2016). In the last two decades, there has been a
decrease in estimates of global lotic N ₂ O evasion (Figure S1), reflecting both lowering EF
estimates and moves towards process-based modeling approaches (Maavara et al. 2019; Yao et
al. 2020; Marzadri et al. 2021). Process-based modeling of aquatic N ₂ O production is especially
warranted because various field studies have shown that N2O evasion rates do not, or only
weakly, correlate with NO ₃ - or TN concentration (Cole and Caraco 2001; Rosamond et al. 2012;
Soued et al. 2016). Moreover, only one upscaling estimate to-date is based on direct
measurements of N_2O in streams or rivers (Soued et al. 2016), reflecting the lack of direct N_2O
measurements and limited understanding of the controls on lotic N ₂ O dynamics.
Spatiotemporal controls on lotic N ₂ O dynamics are poorly understood, which limits
modeling efforts. Spatially, urban (McMahon and Dennehy 1999; Beaulieu et al. 2010, 2011)
and agriculture (Beaulieu et al. 2011; Audet et al. 2017; Mwanake et al. 2019) landcover types
have been associated with high terrestrial nitrogen loading and subsequent high lotic $N_2\mathrm{O}$
emissions. However, a recent study showed that forested rivers have similar NoO concentration

as agriculture rivers (Audet et al. 2020). Further, within-site N₂O concentration and emission variability are difficult to predict. Controls of N₂O dynamics other than, or in addition to, nitrogen include dissolved oxygen (Rosamond et al. 2012), temperature (Beaulieu et al. 2010; Venkiteswaran et al. 2014), and pH (Audet et al. 2020). Even seasonal patterns are not straightforward nor consistent across systems, with some studies showing summer peaks (Beaulieu et al. 2010; Rosamond et al. 2012; Qin et al. 2019), others showing high winter or fall concentrations (Beaulieu et al. 2008; Hama-Aziz et al. 2017; Audet et al. 2020), and still others not detecting consistent seasonal patterns (Cole and Caraco 2001; Stow et al. 2005). This lack of continuous or linear N₂O response to any water quality parameter is reflected in the prevalence of regression tree analysis in field-scale N₂O studies (e.g., Stow et al. 2005; Venkiteswaran et al. 2014; Qin et al. 2019). Taken together, field studies suggest complex interactions between N₂O predictors, which currently contributes to the field's limited understanding of the mechanisms driving N₂O emissions.

The few studies that monitor dissolved N₂O concentration over multiyear timescales find significant interannual variability. For example, a four-year study showed that N₂O concentration in a river in China was an order of magnitude larger in one year compared to the other three years; this interannual variability was much greater than variability attributed to stream order, seasonality, and discharge conditions (Qin et al. 2019). Other time series have also detected higher N₂O concentration and emission rates in dry years, precipitation- or dischargewise, than in wet years (Baulch et al. 2011; Rosamond et al. 2012; Borges et al. 2018). There are, however, exceptions to this wet-year versus dry-year distinction. For example, N₂O concentration was higher during an average summer than a dry summer in the Hudson River (Cole and Caraco 2001). Additionally, a stream with relatively high N₂O concentration showed

an increase in N_2O concentration during a wet year, while two streams with lower N_2O concentration exhibited a decrease (Baulch et al. 2011). In summary, interannual variability in dissolved N_2O concentration is significant, although the mechanisms behind this variability are not yet understood.

In this four-year study, we monitored dissolved N_2O concentration and evasion in eight nested streams and rivers across a temperate forested watershed in the northeast United States. We sampled these eight reaches both regularly and targeting storm events. The main goal of this exploratory study was to assess the dominant sources of variation in N_2O concentration and emission rates in a forested watershed. The study design allowed for assessment of interannual variability, as well as shorter-term variability associated with seasonality and episodic storm events across spatial scales. Here, we contextualize the results of this exploratory research in terms of ecological theory and suggest biogeochemical controls that future work should investigate. Finally, we use these results based on direct N_2O measurements to consider if current modeling approaches have the potential to capture the major sources of variability in N_2O emission rates. These findings have implications for our understanding of lotic N_2O emissions and can inform future modeling efforts.

125 Methods

126 Site descriptions

Eight sites in Connecticut, USA were studied for four consecutive years (2016-2019). The eight study reaches were nested across spatial scales in the Connecticut River Watershed. One study site was located on the Connecticut River mainstem, ~15 km upstream of the Farmington River confluence, while the remaining seven sites were located in the Farmington River subbasin (Figure 1). The Connecticut River starts in Quebec, Canada and has a drainage

basin that includes parts of four New England states (Figure 1). The watershed is predominately forested (Figure 1, Table S1). The Farmington River sub-basin is also predominately forested (Figure 1, Table S1), although the Hartford urban area influences the southeast part of the watershed (Figure 1). Two sites were located on the Farmington River mainstem ~30 km apart; the downstream of these sites (Farmington River 2) was impacted by the Hartford urban area, while the other sites were not. The presence of wastewater treatment plants (WWTPs) reflects this urbanization pattern, with only three WWTPs upstream of Farmington River 1 and an additional five WWTPs upstream of Farmington River 2 (Figure 1).

140 Data collection

Headspace equilibration was used to measure the partial pressure of dissolved N_2O (pN_2O). Grab samples were collected both regularly (~monthly in 2016 and ~twice monthly in 2017-2019) and during high flow events. This sampling strategy allowed for representative coverage of the hydrograph and is described in detail in Aho et al., (2021). Briefly, samples were collected at representative flow exceedance probabilities: a mean of 0.48, a minimum of <0.01, and a maximum of >0.94. All samples were collected in field duplicate from the riverbank. For each sample, a 140-ml syringe was filled with 80 ml of water and 20 ml of N_2 gas and then equilibrated by shaking underwater for 2 min. A 12-ml pre-evacuated Labco Exetainer was filled with 15-ml of the equilibrated headspace until laboratory analysis on a Shimadzu GC2014 or an SRI Model 8610C GC both with electron capture detectors. The gas chromatographs were calibrated with N_2 blanks and 0.251 ppm, 0.951 ppm, 2.5 ppm, and 4.983 ppm certified Airgas N_2O standards. The method detection limit was 0.07 ppm. Precision, calculated as reproducibility of duplicate samples, was \pm 4.4%. Headspace pN_2O was converted

to aqueous pN_2O using Henry's Law and the ideal gas law as was described in Aho and Raymond (2019).

Total dissolved nitrogen (TDN), nitrate (NO₃-), nitrite (NO₂-), and ammonia (NH₄+) concentration data were downloaded from the National Water Information System (NWIS; waterdata.usgs.gov/nwis/). The NWIS data were available for four of the eight study sites: Bunnell Brook, Farmington River 1, Farmington River 2, and the Connecticut River mainstem. Frequency of sampling varied across these four sites, with quarterly measurements available for Farmington River 1, monthly measurements available for Bunnell Brook and Farmington River 2, and twice monthly to weekly measurements available for the Connecticut River mainstem (see Table S1 for data availability summary).

Multiparameter sondes (Eureka Manta 2) were deployed at all sites to measure water temperature, pH, specific conductivity, and dissolved oxygen (DO) at 15-min to 1-hr intervals. Sensors were cleaned twice monthly and pH, DO, and specific conductivity calibrations were checked at least quarterly. During calibration checks, if pH readings were off more than 0.1 pH units, pH sensors were recalibrated using a three-point calibration. If DO readings were off more than the lesser of either 0.3 mg 1⁻¹ or 5%, DO sensors were recalibrated using 100% oxygen saturated water. If specific conductivity readings were off by 5%, conductivity sensors were recalibrated using a one-point calibration. Grab sample data was paired with the nearest-in-time sensor reading.

For seven of the eight sites, 15-min discharge (Q) measurements were collected from NWIS. At the remaining site (Phelps Brook), the USGS gage was inactive and so water stage was measured with a pressure transducer (Hobo U20L) at 15-min to hourly intervals and corrected for barometric pressure. Discharge was calculated with a rating curve based on Q

measurements from flow meter transects and tracer dilutions (Turnipseed and Sauer 2010). Hydrographs for Phelps Brook and Nepaug River are incomplete, starting June 10, 2017 and June 15, 2017, respectively. At each site, the baseflow index (BFI), or the ratio of baseflow to Q, was calculated with the *baseflows()* function from the hydrostats R package (Bond 2019) with mean daily Q and an alpha value of 0.95. This function calculates baseflow using the Lynne-Hollick filter, which is a digital filtering approach (Ladson et al. 2013). The BFI was used to identify and rank hydrologic flow events across the study period for each site. Specific Q was calculated as Q normalized to watershed size. Monthly groundwater table depths from near Bunnell Brook and continuous groundwater table depths from near Hubbard River were also collected from NWIS. Daily rainfall for the Farmington Hydrologic Unit (HUC: 01080207) was collected from the National Oceanic and Atmospheric Administration National Centers for Environmental Information (NOAA CDO).

Calculations and statistical analysis

Evasive N_2O flux rates were calculated as the product of the air-water concentration gradient ($[N_2O]_{water} - [N_2O]_{atm\ equilibrium}$) and the gas transfer velocity (k_{N2O}). Henry's Law was used to convert pN_2O to $[N_2O]$ with temperature-dependent solubility constants (Weiss and Price 1980). A constant atmospheric pN_2O of 0.33 μ atm was used for all calculations based on current atmospheric conditions (CSIRO 2021). The normalized gas transfer velocity (k_{600}) was calculated from water velocity and streambed slope according to *Model Equation 4* from Raymond et al. (2012) and then converted to k_{N2O} with temperature-dependent Schmidt numbers (Wanninkhof 1992). Cumulative emissions were calculated as the product of the duration between measurements and the mean flux of that interval as in Baulch et al. (2011). Finally, the ratio of N found as N_2O and as NO_3^- was calculated. This study conservatively considers the

N₂O:NO₃⁻ ratio a proxy for in-stream nitrogen processing (i.e., representing the proportion of NO₃⁻ converted to N₂O in-stream via incomplete denitrification compared to the remaining NO₃⁻) while other studies have considered this ratio the "concentration method" for calculating EFs (Clough et al. 2011; Outram and Hiscock 2012; Hama-Aziz et al. 2017; Qin et al. 2019). Because samples for N₂O and NO₃⁻ were not collected concurrently, the ratio was calculated from linear interpolation of the data and statistically compared only on the annual scale.

The relationships between water quality parameters and pN_2O were investigated to understand continuous controls on N_2O dynamics. Concentration data was log transformed to approximately meet normality assumptions when required and significance was considered p < 0.05 for parametric tests. Site-specific concentration data were compared visually with violin plots and time-series plots and statistically with linear models using the lm() R function (R Core Team 2020). Synchronicity of pN_2O between sites was examined visually using loess smoothing of time-series data. Seasonality was assessed with boxplots, ANOVA, and post-hoc Tukey multiple comparisons of means. To detect abrupt changes, or change points, in site-specific pN_2O timeseries, we used the WindowSweep() function from the BCPA package (Gurarie et al. 2009; Gurarie 2014), which has been updated to handle irregular, univariate time series (https://github.com/EliGurarie/bcpa/blob/master/inst/doc/bcpa.R). We used a window size of 30 and threshold of 5.

Mixed-effects models accounting for within-site repeated sampling, with site as a random effect, were used to assess environmental controls as fixed effects with the *lmer()* function from the lme4 R package (Bates et al. 2020). All parameters investigated were classified as fixed effects in these models. Intercept was always allowed to vary by site, and slope was also allowed to vary by site when model performance was improved according to the *anova()*

function. First, all physical and chemical correlate variables (i.e., discharge, water temperature, pH, DO, specific conductivity) were included in an initial model to assess environmental controls of pN₂O and assessed by standard errors and for multicollinearity. Then all candidate predictor variables and variables associated with temporal trends (i.e., discharge, water temperature, pH, DO, specific conductivity, date, storm indicator, and one-year post-storm indicator) were included in a model. The one-year post-storm indictor was chosen by assessing temporal trends and testing various post-storm timeframes. Then the *step()* function was used for model selection. As a check, we compared selected model to other model iterations using AIC/BIC, with a preference for BIC because of the explanatory aim of this study, and the anova() function. We checked for potential autocorrelation by running the best model with the lme() function from the nlme R package (Pinheiro et al. 2021) with and without corCAR1 correlation structure assigned. The *anova()* function did not show a difference in performance between the model with and the model without corCAR1 assigned, so we did not account for autocorrelation in these models. All calculations and analysis were completed in R 4.0.2 (R Core Team 2020).

238 Results

223

224

225

226

227

228

229

230

231

232

233

234

235

236

237

239

240

241

242

243

244

245

Partial pressures of N₂O

Here, we report four-years of pN_2O (n = 609) measurements from eight streams and rivers in Connecticut. Across the dataset, the average pN_2O (mean \pm sd) was 0.40 ± 0.20 μ atm (Table 1) with 64% of samples oversaturated compared to atmospheric equilibrium. According to a linear model (log(pN_2O) ~ timestamp + site), the urban-influenced Farmington River site (Farmington River 2) had the highest pN_2O (p < 0.01). Additionally, Nepaug River and the Connecticut River mainstem had significantly higher pN_2O compared to all sites except

Farmington River 2 (p < 0.05, for all sites). All sites, except the urban-influenced Farmington River 2 site, experienced undersaturation, and were therefore sinks of atmospheric N_2O at times (Figure 2). Within site variability was notable, with site-specific coefficients of variation (CVs) varying from 21% to 54%, compared to a CV of 40% for the complete dataset. Taken together, within site variability was significant, with seven of the eight sites exhibiting periods of both N_2O oversaturation and N_2O undersaturation.

No strong correlates (i.e., continuous physical and chemical variables) of pN_2O were identified. Mixed-effects models were used to explore the following correlates on pN_2O : water temperature, specific Q, pH, specific conductivity, and DO. All five variables were weak predictors of pN_2O with large standard errors relative to their estimates (Table S2). Specific Q and DO had negative effects (reported as estimate \pm standard error throughout this section: -0.09 \pm 0.02 and -0.31 \pm 0.11, respectively), while water temperature, pH, and specific conductivity had positive effects (0.009 \pm 0.003, 0.11 \pm 0.06, and 0.26 \pm 0.10, respectively). Seasonality in N_2O saturation was generally very weak and inconsistent across years (Figure S2). Interannual variability, however, was apparent, with the lowest N_2O saturation values occurring in 2018 (Figure S3). This interannual variability is explored in the time-series results to follow.

Time-series analysis

Despite the lack of continuous controls on pN_2O , the time-series data shows synchronicity in pN_2O between all sites except Farmington River 2 (Figure 3a, b). In general, all sites were oversaturated with N_2O from June 2016 until late October 2017, when there was a sharp decline in pN_2O at seven of the sites (Figure 3a). After this decline, all sites except Farmington River 2 showed suppression of pN_2O to below atmospheric equilibrium for an extended period of at least six months (Figure 3a, b). By 2019, pN_2O had generally returned to

oversaturated levels at all sites (Figure 3a, b). Daily rainfall data show an intense precipitation event occurred concurrent with this decline (Figure 3c). In fact, > 14 cm of rain fell on October 30, 2017, making this storm the largest precipitation event of the four-year study (Figure 3c). Taken together, the forested systems, which ranged from small headwaters (<10-km² drainage basin) to the large Connecticut River mainstem (25000-km² drainage basin), showed remarkably similar temporal patterns over the four-year study, including a nearly simultaneous decline from oversaturation to undersaturation during or immediately after an intense rainstorm in late 2017.

269

270

271

272

273

274

275

276

277

278

279

280

281

282

283

284

285

286

287

288

289

290

291

The hydrographs at individual sites can be used to further contextualize pN_2O patterns. River discharge was below average compared to the 20-year record across the watershed during the period of N₂O oversaturation from 2016 until October 2017 (Figure 4, Figure S4). In fact, the 2016 water year had the second lowest flows of the 20-year record at all six sites with active USGS gages and the 2017 water year had the third lowest flows at those same sites except the Connecticut River. The sharp decline in pN_2O in October 2017 (Figure 3a) coincided with precipitation-induced (Figure 3c) high flows at all eight study sites (Figure 4, Figure S4). In terms of absolute flow during the study period, discharges during this storm had very low exceedance probabilities at all sites (0.11% - 1.57%, Figure S5). In terms of baseflow index (BFI), this October 2017 rainstorm was associated with the largest hydrologic events of the study period at all eight sites (Figure 4, Figure S4). Further, it corresponded with elevated groundwater levels at the two sites with groundwater observations (Figure S6). The year following the storm was wetter than the other three study years: 2018 was a typical year for river discharge when compared to the 20-year record across the watershed (Figure 4, Figure S4, Table S3) and the 2018 water year had the 7th-11th lowest annual flows over the 20-year record at the six sites with active USGS gages. Further, the water table remained elevated until the 2019

growing season (Figure S6). In addition, subsequent storms in January 2018, July 2018, and September 2018 were among the top five largest storms for five, five, and four of the study reaches, respectively (Figure 4, Figure S4). In summary, the intense precipitation event on October 30, 2017 (Figure 3c) broke a multiyear dry period and corresponded with a sharp decline in pN_2O to undersaturated levels that were largely maintained throughout the following wet year (Figure 3a, b).

Change-point analysis of site-specific pN₂O time series independently detects a discontinuity following the large October 2017 storm in six of the seven forested systems (Figure 5a, Figure S7). There was a subsequent shift back to oversaturation after 6-12 months at Phelps Brook, Hubbard River, and the Connecticut River mainstem, while a post-storm recovery shift is not detected via change-point analysis at the other forested sites. We returned to mixed-effects models, using date as a fixed effect, to describe the temporal variability in the pN_2O time series. Including the storm as an indicator variable in the mixed-effects models significantly improved performance compared to including only date. Additionally, an indicator variable for one-year post-storm also improved model performance (compared to no post-storm indicator and poststorm timespans of 1 month, 6 months, and 9 months). After considering all candidate predictor variables and using stepwise model selection (Table S4), the best final model (Table 2) shows that the storm indicator is a negative predictor of pN₂O (estimate \pm standard error: -0.48 \pm 0.06), as is the one-year post-storm indicator variable (-0.12 ± 0.03). When the temporal discontinuities are included, pH has a positive effect on pN_2O (0.06 ± 0.02). Model predictions show a sustained decrease in pN_2O for the year following the storm (Figure 6a), which is more obvious when the effects of pH are removed (Figure 6b).

292

293

294

295

296

297

298

299

300

301

302

303

304

305

306

307

308

309

310

311

312

form of inorganic N, accounting for 57 ± 12 % of TDN (data given as mean \pm sd throughout this section). Farmington River 2 had the highest TDN and NO₃-concentrations, followed by Bunnell Brook, the Connecticut River mainstem, and Farmington River 1 (Table 1, Figure S8, p<0.05 for all comparisons). Ammonium concentration was lower, accounting for 9 ± 5 % of TDN. Bunnell Brook and the Connecticut River mainstem had higher NH₄⁺ concentration than the Farmington River sites (Table 1, Figure S8, p<0.05). Time series show that TDN and NO₃ increase after the October 2017 storm in Bunnell Brook (Figure 5b) but not at the other three sites with data (Figure S9). Annual TDN and NO₃ concentrations in the two years before the October 2017 storm and in the two years after were compared (i.e., Nov 2015- Oct 2016; Nov 2016 - Oct 2017; Nov 2017 - Oct 2018; Nov 2018 - Oct 2019). In Bunnell Brook, TDN and NO₃ were significantly higher in the two years after the storm than in the year before the storm (Figure S8, p < 0.05 for both comparisons). Nitrate concentration was significantly higher in 2019 than 2018 for Farmington River 2 and in 2019 than 2016 for the Connecticut River mainstem (Figure S8, p < 0.05 for both). Ammonium concentrations were significantly higher in 2018 than in 2017 for the Connecticut River (Figure S8, p < 0.05). There were no other significant annual differences for the four sites with data (Figure S8). The ratio of N found as N₂O and as NO₃ (i.e., the "concentration method" EF) was calculated (Figure 5c, Figure S10). By site, Farmington River 1 had a higher N₂O:NO₃- ratio across the four-year study (0.0040 ± 0.0012) than the other three sites with NO₃⁻ data $(0.0012 \pm$ 0.0006, 0.0015 ± 0.0008 , and 0.0020 ± 0.0008 for Bunnell Brook, Farmington River 2, and the

Connecticut River mainstem, respectively). Additionally, N₂O:NO₃⁻ ratios were compared one

year before and one year after the large October 2017 storm. At all sites, the pre-storm N₂O:NO₃⁻

For the four sites with dissolved TDN, NO₃, NO₂, and NH₄⁺ data, NO₃ is the dominant

315

316

317

318

319

320

321

322

323

324

325

326

327

328

329

330

331

332

333

334

335

336

ratio was significantly higher than the post-storm ratio (p<<0.01). At Bunnell Brook, the post-storm N_2O : NO_3^- ratio (0.0009 \pm 0.0002) was less than half of the pre-storm ratio (0.0019 \pm 0.0004). At Farmington River 1, the pre- and post-storm ratios were 0.0044 \pm 0.0006 and 0.0032 \pm 0.0008, respectively and at Farmington River 2, the pre- and post-storm ratios were 0.0021 \pm 0.0013 and 0.0013 \pm 0.0006, respectively. Finally, the pre- and post-storm ratios in the Connecticut River mainstem were 0.0025 \pm 0.0010 and 0.0017 \pm 0.0005, respectively. In summary, Farmington River 1, the site with the lowest NO_3^- concentration, had the highest $N_2O:NO_3^-$ ratio, and all sites had higher pre-storm than post-storm $N_2O:NO_3^-$ ratios, although this difference was strongest in Bunnell Brook.

 N_2O emissions

Across the four-year study, all sites were net sources of N₂O to the atmosphere, although there was considerable interannual variability. Evasive fluxes peaked in 2017 and were their lowest in 2018 (Figure 5d, Figure S11). Timeseries show a shift from positive to negative evasive fluxes after the October 2017 storm at all sites except Farmington River 2 (Figure 5d, Figure S11). Evasive fluxes integrated over time show that net annual emissions were positive for 2016, 2017, and 2019 for all sites with data (Figure 7). Five sites had negative emissions for 2018, meaning they were net annual sinks of N₂O (Figure 7). Evasive fluxes were not calculated for 2016 nor 2017 in Phelps Brook and Nepaug River because of the lack of discharge data (Figure 7). In sum, interannual variability in N₂O evasion was high, with most of the study systems switching from N₂O sources to N₂O sinks following the large October 2017 storm.

358 Discussion

The N₂O concentration and flux data reported in this study are generally within the ranges of prior lotic N_2O studies. To facilitate comparison with other studies, the mean \pm standard deviation of N₂O saturation in this study is $134 \pm 66\%$, which is equivalent to pN₂O of 0.40 ± 0.20 µatm and a N₂O concentration of 0.43 ± 0.25 µg-N l⁻¹. Additionally, the mean \pm standard deviation of evasive flux rates is 0.81 ± 2.7 mg-N m⁻² d⁻¹. Average N₂O concentration in this study is similar to those of three of four rivers in Belgium (127-197% saturation, Borges et al., 2018) and the Congo River watershed (142% saturation, Borges et al. 2019); and N₂O diffusive flux rates in this study are similar to agriculture headwater streams in Michigan (0.84 mg-N m⁻² d⁻¹, Beaulieu et al. 2008). On the other hand, this study reports higher N₂O concentration than a river in New Zealand (114% saturation, Clough et al. 2011) and African rivers in general (0.26 µg-N l⁻¹, Borges et al. 2015), and higher N₂O fluxes than a coastal watershed in North Carolina (0.31 mg-N m⁻² d⁻¹, Stow et al. 2005), rivers on the Tibetan Plateau (0.18 mg-N m⁻² d⁻¹, Qu et al. 2017), and boreal rivers (0.05 mg-N m⁻² d⁻¹, Soued et al. 2016). However, our average N₂O concentration is lower than nearby first-order streams in Connecticut (0.63 μ atm, Aho and Raymond 2019), forested (1.6 \pm 2.1 μ g-N l⁻¹) and agriculture (1.3 \pm 1.8 μ g-N l⁻¹) streams in Sweden (Audet et al. 2020), and agriculture-influenced rivers in Kenya (0.51 μg-N l⁻¹, Mwanake et al. 2019), Belgium (1406%, Borges et al. 2018), and the Upper Mississippi River (250%, Turner et al. 2016). In summary, the forested watershed in this study had moderate N₂O concentration and fluxes compared to global rivers and streams of various land uses and land covers, with values higher than boreal and alpine watersheds but lower than many headwater streams and agriculture-influenced systems. In this study, the urban-influenced site was the exception, exhibiting significantly higher

N₂O concentration and emission rates than the other seven study sites. Nitrous oxide

360

361

362

363

364

365

366

367

368

369

370

371

372

373

374

375

376

377

378

379

380

381

concentration was about twice as high at the Farmington River 2 site as in the other seven sites. Additionally, the Farmington River 2 site was the only site to be a constant N₂O source to the atmosphere. The Farmington River 2 site is influenced by different land use and land cover relative to the other forested sites even though it is located only ~15 km downstream of the Farmington River 1 site. There are eight WWTPs in the drainage basin of the Farmington River 2 site compared to just three for the Farmington River 1 site. Further, the Farmington River 2 site is influenced by the Hartford urban area and its drainage basin has about twice the developed area as the upstream Farmington River 1 site (Figure 1, Table S1). Elevated N₂O concentration is likely attributable to increased urbanization and WWTP inputs because WWTP nutrient removal processes produce significant amounts of nitrogen species, including N₂O (Massara et al. 2017), and WWTP effluent is a source of denitrifying bacteria to streams and rivers (Rahm et al. 2016). This pattern is in agreement with prior studies as N₂O peaks have been reported downstream of WWTPs (Beaulieu et al. 2010; Rosamond et al. 2012). Further, urban landcover, in general, is associated with high N_2O fluxes (Beaulieu et al. 2011). Our study supports the idea that urban rivers are sources of N₂O to the atmosphere due to anthropogenic N loading.

383

384

385

386

387

388

389

390

391

392

393

394

395

396

397

398

399

400

401

402

403

404

405

Abrupt change in pN₂O

There was a sudden shift in pN_2O and N_2O emission rates in the forested reaches corresponding to a large rainstorm mid-way through our study. From 2016 until October 2017, when pN_2O and N_2O emission rates were elevated at all sites, the watershed was drier than average. The Farmington River watershed experienced periods of extreme drought in 2016 and 2017 (National Drought Mitigation Center 2020) and all sites experienced lower-than-average flow conditions for most of 2016 and 2017 (Figure 4, Figure S4, Table S3). The nearly two-year dry period was broken by an intense rainstorm in late October 2017 (Figure 3b), which was

associated with high discharges at all sites (Figure 4, Figure S4) and a sharp decline from N_2O oversaturation to undersaturation in seven of the eight study sites (Figure 3a). Results indicate that this sharp decline in pN_2O was followed by a prolonged period of low pN_2O at the majority of sites (Figure 3a, b). To our knowledge, similar abrupt and sustained shifts have not been previously reported, possibly due to the limited number of multiyear N_2O time series. However, other studies have reported higher N_2O concentration during drier years than wetter years (Baulch et al. 2011; Rosamond et al. 2012; Borges et al. 2018), although the opposite has also been shown (Cole and Caraco 2001; Baulch et al. 2011). Considering the lack of strong continuous controls (e.g., specific Q, water temperature, specific conductivity, and DO) on pN_2O , the sudden shift in N_2O dynamics coincident with the large precipitation event appears to have been the largest source of N_2O variability in the study system over the four-year study period.

Annual climatology may have acted as an interaction, amplifying the impact of the storm. In other words, the 2016-2017 dry period may have resulted in elevated pN_2O before the storm and the sustained wet conditions in 2018 may have continued to suppress N_2O production contributing to an extended recovery. Such interactions between stream drying and flooding are known to amplify the biotic impacts of disturbance (Stanley et al. 2010). The large October 2017 storm not only significantly increased discharge at all sites, but also caused overall hydrologic conditions to change. The storm was associated with elevated water tables throughout the watershed, which then remained elevated throughout 2018 (Figure S6), and was followed by additional large hydrologic flow events throughout 2018 (Figure 4, Figure S4). This overall shift in hydrologic conditions in the year following the storm may have induced a state change both hydrologically and for N_2O processes on the annual scale. This study cannot

disentangle the effects of the pre-storm dry period and the post-storm wet year on the N₂O response to the large storm, but it seems possible that the dry period primed the watershed to be less resistant to disturbance and the post-storm wet year reduced the resilience (Boesch 1974) of the system, suppressing or slowing recovery of pre-storm N₂O conditions. Regardless, results show that this particular hydrologic event triggered a threshold response that smaller hydrologic events did not. In sum, we attribute the sudden shift in N₂O dynamics to the late October 2017 rainstorm that broke a prolonged dry period, although other aspects of annual climatology likely exacerbated the effect.

These potential interactions lead to the question: was the sustained period of undersaturation following the October 2017 storm due to a regime shift or a slow recovery to N₂O oversaturation? Evidence for a new state in the months following the large storm include the significance of a one-year post-storm indicator variable in the best mixed-effect model describing the dataset (Table 2, Figure 6) and the change points detected 6-12 months post-storm in the time-series data from Phelps Brook, Hubbard River, and the Connecticut River mainstem (Figure S7). These lines of evidence support the idea that the storm caused a new state in N₂O dynamics in the post-storm year. However, classifying this response as a regime shift (Holling 1973; Folke et al. 2004) would require identification of positive feedback mechanisms and multivariate responses, which is beyond the scope of this descriptive study. The detection of two abrupt changes in the data (immediately post-storm and 6-12 months post-storm) does allow us to categorize the storm response in N₂O dynamics an "abrupt but temporary" response (Ratajczak et al. 2018). However, further confounding the abrupt change classification is the ~linear post-storm recovery trends apparent in Bunnell Brook, Nepaug River, Still River, and

Farmington River 1 (Figure 5 and S7). In sum, our results indicate that both a sustained shift and recovery trend are possible, and perhaps worked together, to create the pN_2O dynamics reported.

451

452

453

454

455

456

457

458

459

460

461

462

463

464

465

466

467

468

469

470

471

472

473

Regardless of post-disturbance classification, the large hydrologic event seemed to push forested reaches across watershed scales from consistent N2O sources to prolonged N2O sinks on an annual basis. This sustained period of N₂O undersaturation had implications for annual emissions, resulting in net negative evasion for 2018 at fives of the eight study sites. This switch from N₂O source to N₂O sink on annual scales was surprising, especially given the continued availability of NO₃⁻ for in-stream processing, eliminating the possibility that NO₃⁻ availability limited N₂O production. Emission estimates based on EFs assume that a static percentage of DIN inputs is converted to N₂O (e.g., Seitzinger and Kroeze 1998; Hu et al. 2016). The nonlinear N₂O response reported here strongly challenges this assumption, given the post-storm N₂O:NO₃⁻ ratios were 29-59% lower than the pre-storm N₂O:NO₃⁻ ratios at sites with available data. Additionally, process-based models based on water residence time (e.g., Marzadri et al. 2017; Maavara et al. 2019) would also miss this type of abrupt shift in emissions, given the nonlinear response to discharge. In this study, sustained N₂O undersaturation significantly mitigated emissions during this four-year study, suggesting the importance of extreme hydrologic events and prolonged undersaturation to lotic N₂O emission estimates.

Potential mechanisms controlling N_2O production and consumption

In general, incomplete denitrification in streambed sediments is thought to be the dominant pathway for N₂O production in streams and rivers globally (Marzadri et al. 2017; Quick et al. 2019). Denitrification reduces NO₃⁻ to N₂ gas via a redox sequence that includes N₂O as an intermediatory, and the hyporheic zone is a denitrification "hotspot" because oxic NO₃⁻-rich surface water converges with a reducing environment (McClain et al. 2003; Gomez-

Velez et al. 2015). Our study seems to reflect the literature consensus that incomplete denitrification is largely responsible for N₂O production given the relatively high NO₃⁻ concentration compared to NH₄⁺ concentration; although, nitrification and nitrifier-denitrification, which consume NH₄⁺, cannot be ruled out given the low NH₄⁺ concentration. Additionally, the relatively high DO and low turbidity levels in this study (Table 1) would likely inhibit denitrification on anoxic microsites in the water column (Liu et al., 2013; Reisinger et al., 2016; Xia et al., 2017), suggesting the benthic and hyporheic zones would be more favorable locations for N₂O production. However, the synchronicity across spatial scales leads us to also consider the potential for catchment-scale controls on lotic *p*N₂O.

In-stream processes

If sediment-zone denitrification is the dominant production pathway, the rate of N₂O production would be determined by two factors: hydrologic residence time and biogeochemical reaction rates (Quick et al. 2016; Marzadri et al. 2017). Substantial biofilm presence has the potential to support elevated N₂O production by increasing water residence time in the hyporheic zone (Caruso et al. 2017; Newcomer et al. 2018) and supporting large denitrifying bacteria populations (Nielsen et al. 1990; Peterson et al. 2011). Without major disturbance events, the hyporheic zone can become a location of stable biofilm growth and accrual, which supports strong biogeochemical interfaces that may induce denitrification (Battin et al. 2016; Caruso et al. 2017; Roy Chowdhury et al. 2020) and could have supported N₂O production in the first half of this study. Large hydrologic events, like that stemming from the October 2017 rainstorm, disturb sediments and biofilm via physical scouring and burial (Fisher et al. 1982; O'Connor et al. 2012; Robinson et al. 2018), resulting in shorter water residence times and disturbance of denitrifying microbial communities. These conditions may have been maintained by the occurrence of

several more significant hydrologic events in the next water year, supporting the sustained low pN_2O in 2018 (Figure 4, Figure S4). Finally, elevated water tables in 2018 could result in a contraction of the hyporheic zone (Boano et al. 2014), further reducing potential sediment-zone denitrification. These potential sediment-zone mechanisms, based on current framework of N_2O controls in the literature, are summarized in Figure 8 and future studies should evaluate their potential to support abrupt changes in N_2O dynamics.

Catchment processes

497

498

499

500

501

502

503

504

505

506

507

508

509

510

511

512

513

514

515

516

517

518

519

However, our finding of watershed-scale synchronicity in N₂O dynamics suggests that catchment-scale processes might also be important controls of N₂O dynamics. Beyond the stream channel, watershed-scale hydrologic conditions can rapidly change during storm events. For instance, altered water tables and activated flow paths can result in the rerouting of water and solutes to denitrification hotspots and control points (McClain et al. 2003; Bernhardt et al. 2017; Covino et al. 2018) and the reduction of water residence time (Jencso et al. 2009) in the riparian zone. These emergent watershed-scale processes and their control on stream N₂O conditions are not yet well documented but have the potential to explain the concurrent changes in watershedscale hydrologic conditions and prolonged storm impacts on pN₂O undersaturation. Low water tables, like those that occurred during the 2016-2017 dry period and in 2019, could increase the total area supporting denitrification through the routing of water through riparian zones before reaching the channel (Jencso et al. 2009). This catchment-scale control could also explain why the urban system did not experience the sharp and sustained decline in N₂O like the forested sites. The N₂O dynamics of the urban reach were likely controlled by direct inputs of N₂O and denitrifying bacteria from the numerous WWTPs in its drainage basin (Rahm et al. 2016; Massara et al. 2017), rather than natural flow paths subject to hydrologic rerouting and

activation. The synchronicity in pN_2O across forested reaches strongly suggests the importance of catchment-scale processes, such as riparian production, in controlling stream and river N_2O dynamics.

*N*₂*O* consumption processes

520

521

522

523

524

525

526

527

528

529

530

531

532

533

534

535

536

537

538

539

540

541

542

Regardless of the dominance of local or distal N₂O production during periods of N₂O oversaturation (2016-Oct 2017 and 2019), N₂O consumption processes must also be considered to explain the length period of post-storm N₂O undersaturation. Undersaturation implies that sink processes, such as complete denitrification of N₂O to N₂, outpace the rate of atmospheric N₂O invasion across the air-water boundary. The occurrence of nitrous oxide undersaturation in rivers has previously been reported (e.g., Baulch et al. 2011; Soued et al. 2016; Borges et al. 2019), although responsible mechanisms remain largely hypothetical. Environmental conditions associated with N₂O undersaturation include low NO₃, high dissolved organic carbon, and low DO (Baulch et al. 2011; Soued et al. 2016; Borges et al. 2019) as these factors support complete denitrification of N₂O to N₂. In our study, terrestrial DOC inputs were likely higher in 2018 due to higher discharge and terrestrial flushing (Raymond et al. 2016), especially in streams and smaller rivers (Hosen et al. 2020). However, the abrupt shift from oversaturation to undersaturation suggests that N₂O undersaturation may be a threshold response to extreme weather events rather than just supported by specific environmental conditions. In sum, if N₂O conversion to N₂ increased in 2018 or if in-stream consumption rates were simply not masked by riparian N₂O inputs remains an open question.

Instantaneous storm processes

Although much of this section has been to dedicated mechanisms that could explain the sustained shift in pN_2O , instantaneous storm responses are also apparent in our data. Two sites

(Phelps Brook and Nepaug River) exhibited a peak in pN_2O during the October 2017 storm that was not sustained post-storm. These peaks may have been the result of hyporheic-zone flushing; an idea that is supported by a recent modeling study predicting a pulse of dissolved N_2 after a precipitation event reconnects a stream to its hyporheic zone (Newcomer et al. 2018), suggesting N_2O gas could experience the same dynamic. Although grab sampling did not capture similar peaks at the other sites, all forested sites experience post-storm N_2O dilution. Both flood dilution (Webb et al. 2017) and general source limitation (e.g., Moatar et al. 2017) may explain the immediate post-storm decline in pN_2O . Further, many studies of other dissolved gases report decreases with event flows both in the Connecticut River watershed (Aho and Raymond 2019; Aho et al. 2021) and beyond (e.g., Billett and Harvey 2013; Crawford et al. 2013; Looman et al. 2016). However, given the grab-sampling methodology used, this study provides more insights into long-term rather than instantaneous storm dynamics.

Conclusion

This four-year study of lotic *p*N₂O and N₂O emission rates documents a non-linear response in N₂O dynamics in forested streams and rivers after a large precipitation event. This study adds to existing literature on the effects of hydrologic disturbance on lotic nitrogen cycling (e.g., Grimm 1987; Marti et al. 1997), and documents the importance of hydrologic disturbance on lotic N₂O emissions. Of particular interest to future observation and modeling studies is how to capture and represent lengthy state change in net N₂O source-sink processes, such as the 6- to 12-month periods of N₂O undersaturation reported here. Although the effects of watershed-scale hydrology on N₂O production have received little attention to date, the results presented here suggest that watershed-scale drivers of N₂O production may warrant attention, in addition to instream mechanisms that currently are the focus of emissions models. This study illustrates that

566 lotic N₂O evasion experiences nonlinear storm responses, which highlights the need to identify 567 and model such abrupt changes in lotic N₂O production and emissions. 568 Acknowledgments, Samples, and Data 569 This project was supported by NSF Award 1340749, NASA Award NNX17AI74G, NASA 570 Connecticut Space Grant Consortium Graduate Research Fellowship, Yale Analytical and Stable 571 Isotope Center, and Yale Institute for Biospheric Studies. We thank Bob Hall, Eli Fenichel, and 572 Stephanie Weber for their helpful suggestions on the analysis. Data will be available online at 573 Environmental Data Initiative upon acceptance. 574 **Author contributions** 575 KA and PR conceptualized the study design. KA, JF, JH, EK, LL, LW, BY, and PR designed the 576 nested catchment framework, including site selection, site infrastructure, probe 577 deployment/maintenance, and stream gaging, and performed fieldwork. JZ contributed to data 578 analysis and interpretation. PR oversaw all work, including data collection, data analysis, and 579 writing. KA analyzed the dataset and wrote the manuscript with input from all authors. 580 **Conflicts of interest** 581 The authors have no conflicts of interest to disclose. 582 583

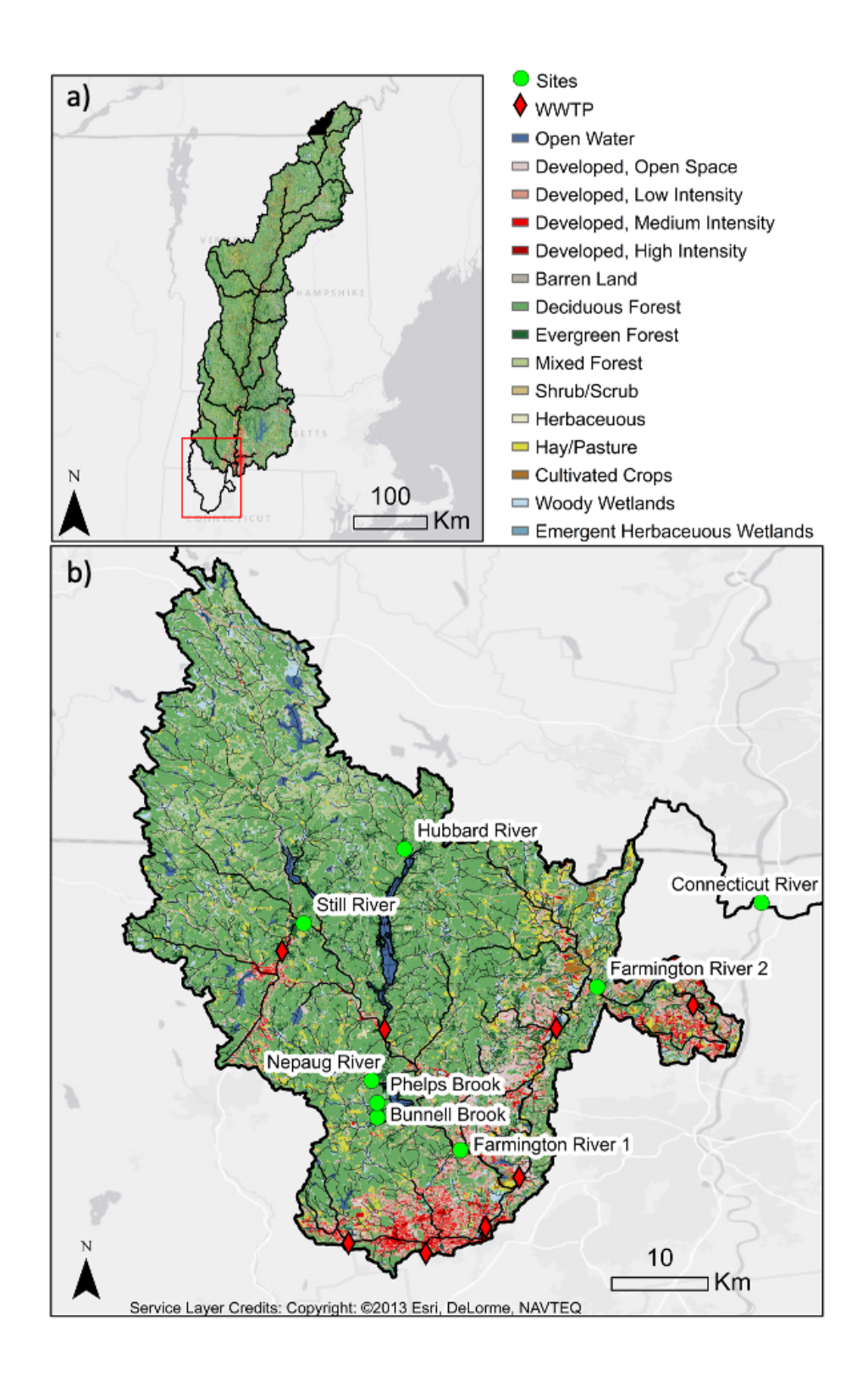


Figure 1. Map of the study area showing a) the Connecticut River watershed and b) the location of the Farmington River watershed in the region. Stream network is from National Hydrography

Dataset Plus High Resolution (NHDPlus HR), landcover data is from National Land Cover

Database (NLCD 2011), and the locations of wastewater treatment plants (WWTPs) are from the

Environmental Protection Agency Facility Registry (EPA FRS).

Table 1. Mean ± standard deviation of measured water chemistry variables, where DO is

Table 1. Mean ± standard deviation of measured water chemistry variables, where DO is dissolved oxygen, SpCond is specific conductivity, Turb is turbidity, TDN is total dissolved nitrogen, NO₃⁻ is nitrate, NO₂⁻ is nitrite, and NH₄⁺ is ammonium.

Site	pN ₂ O (μatm)	рН	DO (mg l ⁻¹)	SpCond (μS cm)	Turb (NTU)	TDN (mg-N l ⁻¹)	NO ₃ - (mg-N l ⁻¹)	NO ₂ - (mg-N l ⁻¹)	NH ₄ ⁺ (mg-N l ⁻¹)
Phelps Brook	0.33 ± 0.10	6.4 ± 0.3	9.5 ± 2.1	97 ± 21	8.3 ± 9.7	n.d.	n.d.	n.d.	n.d.
Bunnell Brook	0.35 ± 0.09	7.0 ± 0.2	10.3 ± 1.7	172 ± 33	7.4 ± 13.8	0.58 ± 0.10	0.35 ± 0.13	0.003 ± 0.002	0.06 ± 0.04
Hubbard River	0.30 ± 0.08	6.7 ± 0.3	11.0 ± 2.2	51 ± 15	1.2 ± 2.1	n.d.	n.d.	n.d.	n.d.
Nepaug River	0.40 ± 0.09	6.9 ± 0.2	10.4 ± 1.9	116 ± 26	12.9 ± 19.4	n.d.	n.d.	n.d.	n.d.
Still River	0.34 ± 0.09	7.6 ± 0.3	10.7 ± 1.8	209 ± 64	9.1 ± 10.9	n.d.	n.d.	n.d.	n.d.
Farmington River 1	0.37 ± 0.10	7.4 ± 0.5	10.9 ± 1.7	124 ± 40	4.4 ± 5.1	0.28 ± 0.05	0.11 ± 0.03	0.002 ± 0.001	0.02 ± 0.01
Farmington River 2	0.72 ± 0.39	6.8 ± 0.2	10.3 ± 2.0	210 ± 46	8.0 ± 11.1	0.77 ± 0.18	0.53 ± 0.17	0.007 ± 0.006	0.03 ± 0.01
Connecticut River	0.46 ± 0.14	6.8 ± 1.1	11.0 ± 2.5	150 ± 34	11.4 ± 13.5	0.50 ± 0.10	0.27 ± 0.07	0.004 ± 0.002	0.05 ± 0.02

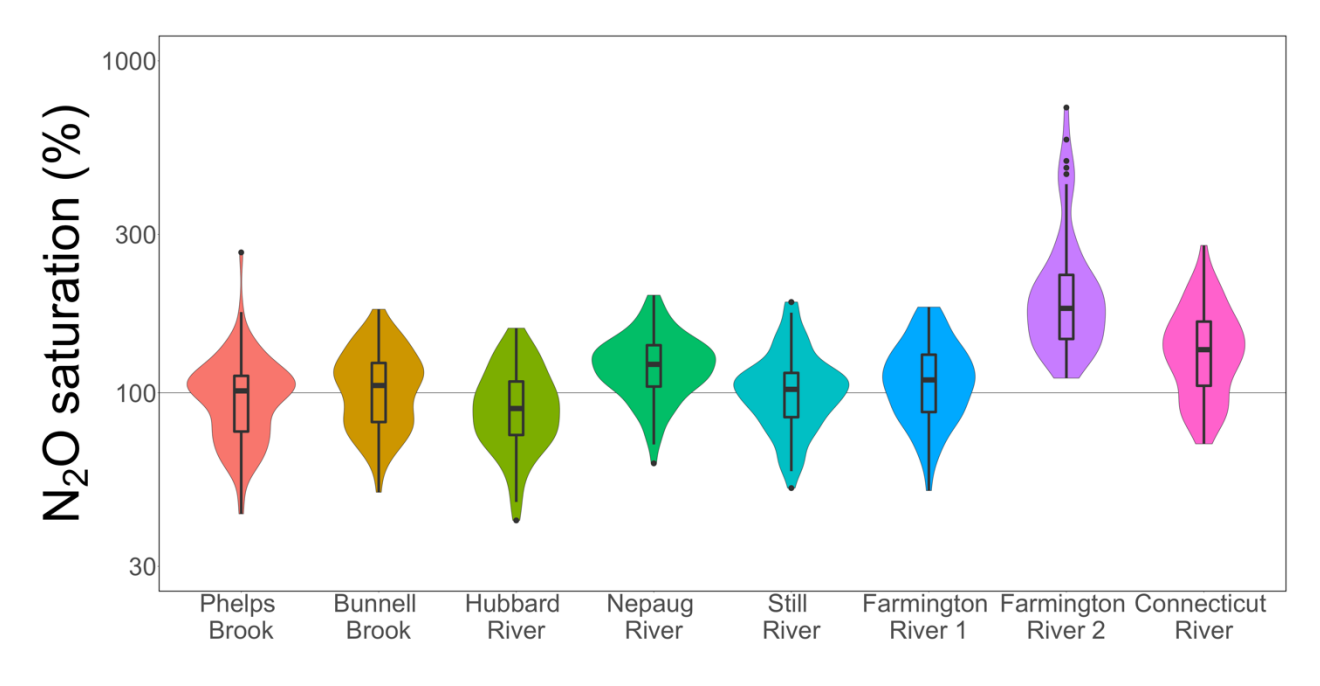


Figure 2. Violin plots of N_2O saturation by site with embedded boxplots, where boxes represent the median and interquartile range (IQR), whiskers mark the lesser of 1.5 x IQR or minimum/maximum, and points denote outliers more extreme than 1.5 x IQR. A saturation of 100% implies atmospheric equilibrium. Sites are arranged from left to right in order of drainage area. The y-axis is log transformed.

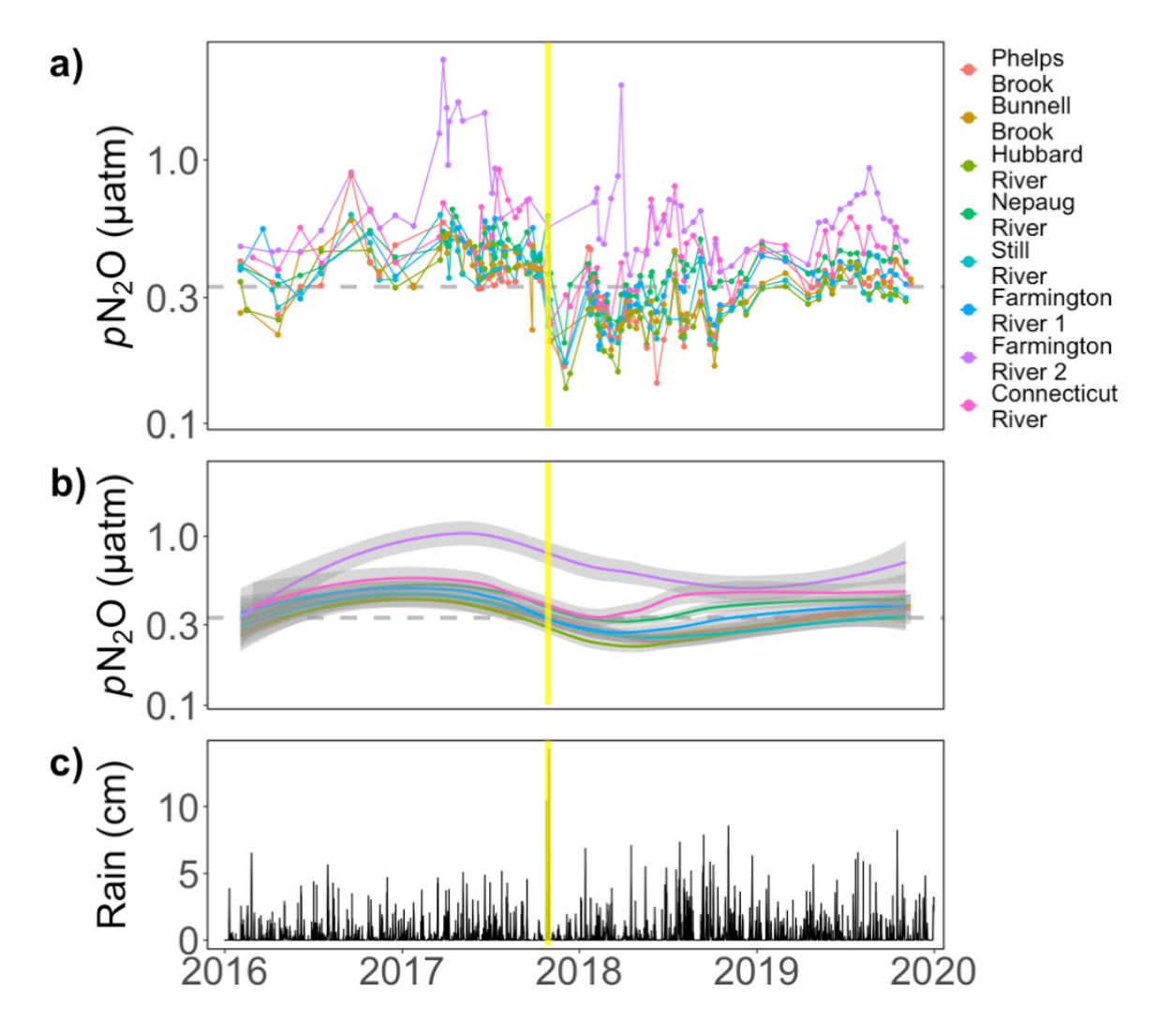


Figure 3. Variability in pN_2O and rainfall through time over the four-year study. Part a) shows timeseries of pN_2O for all eight study sites. The grey dashed line represents atmospheric equilibrium. Part b) shows loess smoothing of the pN_2O time series for all eight sites. Part c) shows a hyetograph showing daily rainfall in the Farmington Hydrologic Unit (HUC: 01080207) from the National Oceanic and Atmospheric Administration National Centers for Environmental Information (NOAA CDO). On all subplots, the yellow vertical line marks the largest storm event during the study in terms of baseflow index, which corresponds with the highest rainfall intensity of the study period.

Bunnell Brook

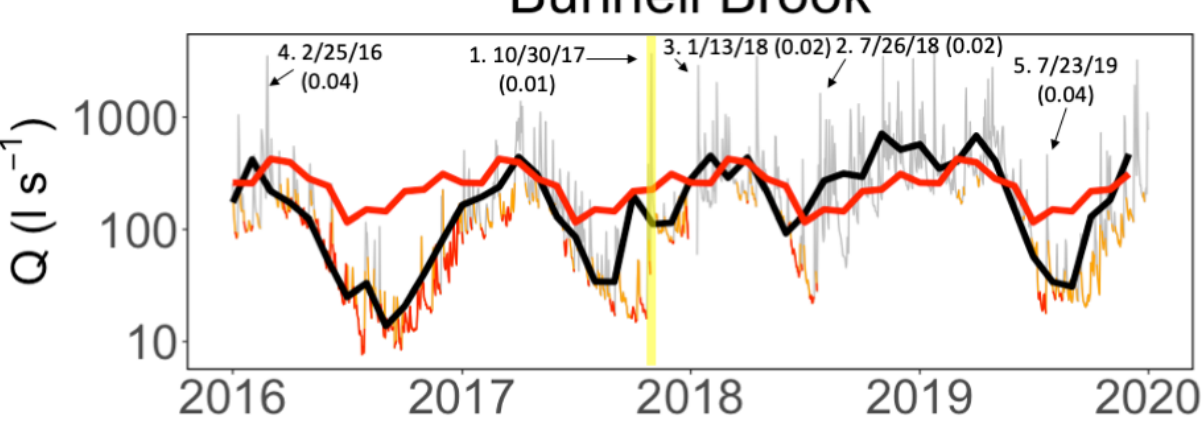


Figure 4. A hydrograph of mean daily discharge (Q) at Bunnell Brook. Note the log-transformed y-axis. The hydrograph (in grey) is colored orange when Q is below the 50th flow percentile for that day over a 20-year period (2000-2019) and red when Q is below the 20th flow percentile. The bold black line is the smoothed hydrograph, which uses mean monthly Q, while the bold red line is mean monthly Q for the 20-year period. The five largest hydrologic events, in terms of baseflow index values, are labeled with rank, date, and baseflow index. In addition, the large October 2017 storm is highlighted in yellow. See Figure S4 for the remaining sites.

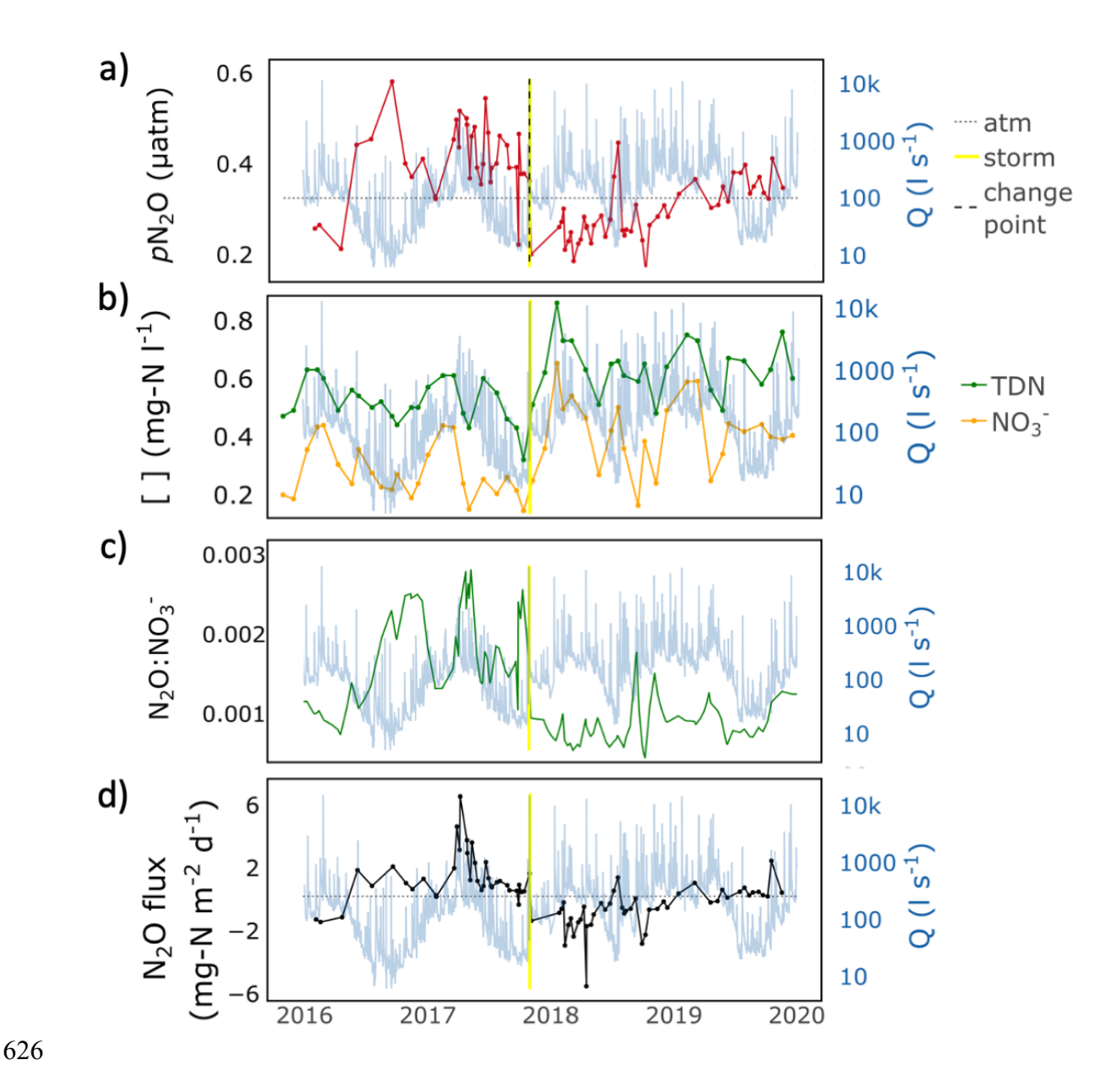


Figure 5. Timeseries of (a) pN_2O , (b) TDN and NO_3^- concentration, (c) the ratio of linearly interpolated N found as N_2O and as NO_3^- (i.e., the "concentration method" EF), and (d) N_2O evasive fluxes from Bunnell Brook, a representative forested system. The other seven timeseries of pN_2O and N_2O emissions are in the SI. The other three timeseries for TDN, NO_3^- , and N_2O : NO_3^- are also located in the SI. For the pN_2O timeseries (a), discontinuities detected by changepoint analysis are plotted as black dashed lines and atmospheric pN_2O is indicated by the grey

dashed line. The largest hydrologic event of this study (in terms of baseflow index), which was associated with the intense precipitation event on October 30, 2017, is highlighted in yellow.

Table 2. Table summarizing the best mixed-effect model of pN_2O (μ atm). Fixed effects are given as an estimate, standard error (SE), and 95% confidence interval (95% CI).

Model: $log(pN_2O) \sim date + storm indicator + 1-year post-storm indicator + pH + (1 site)$					
	Estimate	SE	95% CI		
Intercept	-1.33	0.18	(-1.680.99)		
Date	0.0003	0.00006	(0.0002 - 0.0005)		
Storm indicator	-0.48	0.06	(-0.580.37)		
1-yr post-storm indicator	-0.12	0.03	(-0.180.06)		
рН	0.06	0.02	(0.02 - 0.11)		

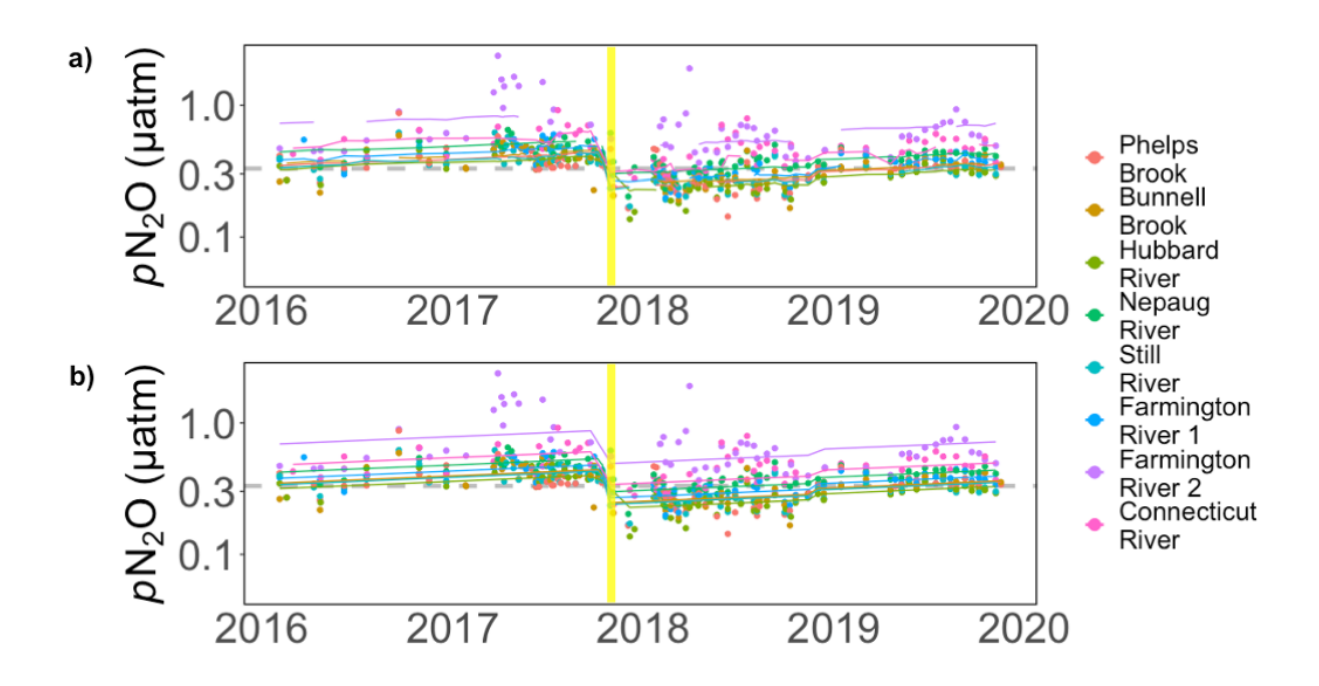


Figure 6. Part a) shows predictions from the mixed-effect model as lines and measured pN_2O as points for all eight study sites. Part b) shows predictions from the mixed-effect model, when pH is excluded, as lines to highlight the temporal dynamics and measured pN_2O as points for all

eight study sites. On both subplots, the grey dashed line represents atmospheric equilibrium, and the yellow vertical line marks the large October 2017 storm.

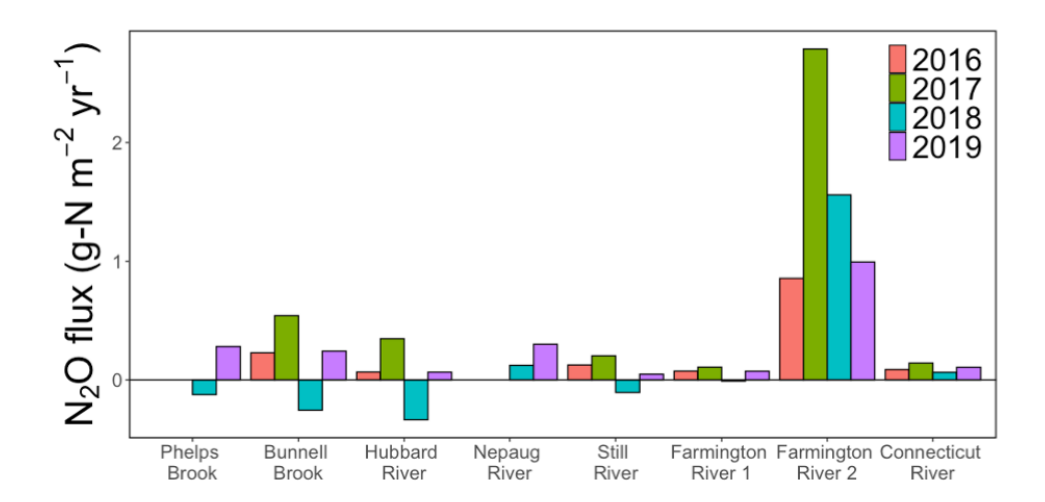


Figure 7. Annual evasive N_2O fluxes by site. Phelps Brook and Nepaug River fluxes are only available starting in July 2017 and so there are no annual estimates for 2016 nor 2017.

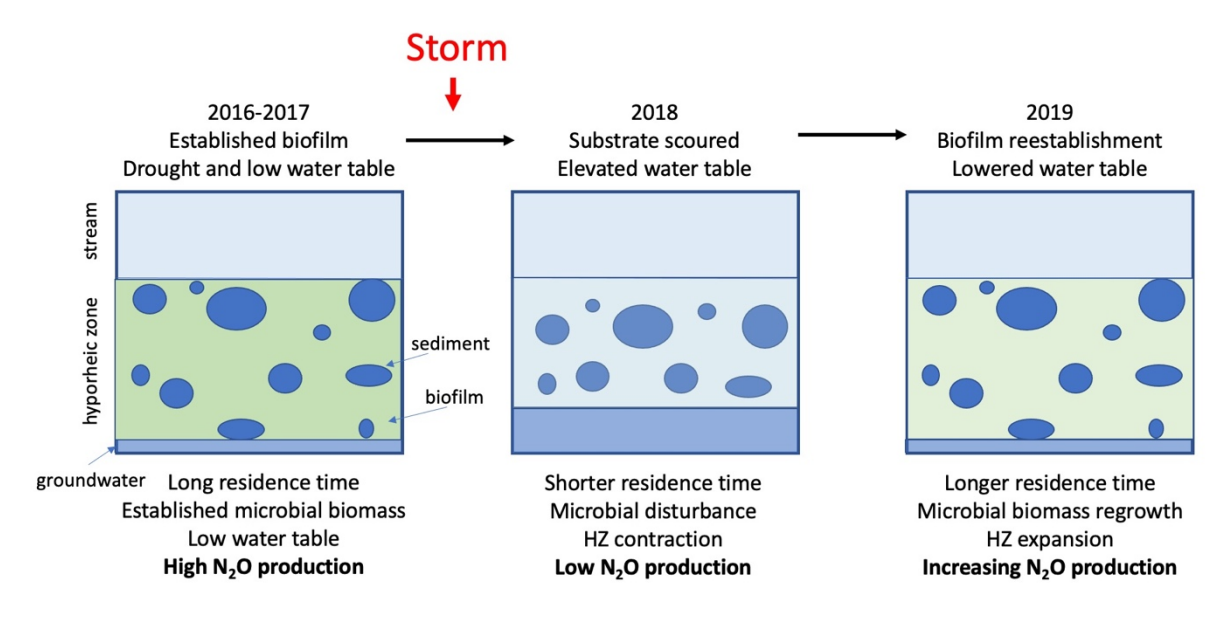


Figure 8. Conceptual diagram summarizing potential in-stream processes controlling N_2O production. Here HZ denotes hyporheic zone.

- Aho, K. S., J. H. Fair, J. D. Hosen, and others. 2021. Distinct concentration-discharge dynamics
- in temperate streams and rivers: CO₂ exhibits chemostasis while CH₄ exhibits source
- limitation due to temperature control. Limnol. Oceanogr. lno.11906. doi:10.1002/lno.11906
- Aho, K. S., and P. A. Raymond. 2019. Differential Response of Greenhouse Gas Evasion to
- Storms in Forested and Wetland Streams. J. Geophys. Res. Biogeosciences 649–662.
- doi:10.1029/2018jg004750
- Audet, J., D. Bastviken, M. Bundschuh, and others. 2020. Forest streams are important sources
- for nitrous oxide emissions. Glob. Chang. Biol. **26**: 629–641. doi:10.1111/gcb.14812
- Audet, J., M. B. Wallin, K. Kyllmar, S. Andersson, and K. Bishop. 2017. Nitrous oxide
- 660 emissions from streams in a Swedish agricultural catchment. Agric. Ecosyst. Environ. 236:
- 661 295–303. doi:10.1016/j.agee.2016.12.012
- Bates, D., M. Maechler, B. Bolker, and others. 2020. lme4: Linear Mixed-Effects Models using
- "Eigen" and S4. version 1.1-23.
- Battin, T. J., K. Besemer, M. M. Bengtsson, A. M. Romani, and A. I. Packmann. 2016. The
- ecology and biogeochemistry of stream biofilms. Nat. Rev. Microbiol. 14: 251–263.
- doi:10.1038/nrmicro.2016.15
- Baulch, H. M., S. L. Schiff, R. Maranger, and P. J. Dillon. 2011. Nitrogen enrichment and the
- emission of nitrous oxide from streams. Global Biogeochem. Cycles 25: n/a-n/a.
- doi:10.1029/2011GB004047
- Beaulieu, J. J., C. P. Arango, S. K. Hamilton, and J. L. Tank. 2008. The production and emission
- of nitrous oxide from headwater streams in the Midwestern United States. Glob. Chang.
- 672 Biol. **14**: 878–894. doi:10.1111/j.1365-2486.2007.01485.x
- Beaulieu, J. J., W. D. Shuster, and J. A. Rebholz. 2010. Nitrous oxide emissions from a large,

- impounded river: The Ohio river. Environ. Sci. Technol. 44: 7527–7533.
- doi:10.1021/es1016735
- Beaulieu, J. J., J. L. Tank, S. K. Hamilton, and others. 2011. Nitrous oxide emission from
- denitrification in stream and river networks. Proc. Natl. Acad. Sci. **108**: 214–219.
- doi:10.1073/pnas.1011464108
- Bernhardt, E. S., J. R. Blaszczak, C. D. Ficken, M. L. Fork, K. E. Kaiser, and E. C. Seybold.
- 680 2017. Control Points in Ecosystems: Moving Beyond the Hot Spot Hot Moment Concept.
- 681 Ecosystems **20**: 665–682. doi:10.1007/s10021-016-0103-y
- Billett, M. F., and F. H. Harvey. 2013. Measurements of CO₂ and CH₄ evasion from UK peatland
- headwater streams. Biogeochemistry **114**: 165–181. doi:10.1007/s10533-012-9798-9
- Boano, F., J. W. Harvey, A. Marion, A. I. Packman, R. Revelli, L. Ridolfi, and A. Wörman.
- 685 2014. Hyporheic flow and transport processes: Mechanisms, models, and biogeochemical
- implications. Rev. Geophys. **52**: 603–679. doi:10.1002/2012RG000417
- Boesch, D. F. 1974. Diversity, stability and response to human disturbance in estuarine
- 688 ecosystems. Proc. First Int. Congr. Ecol. **Structure**,: 109–114.
- Bond, N. 2019. hydrostats: Hydrologic Indices for Daily Time Series. version: 0.2.7.
- Borges, A. V., F. Darchambeau, T. Lambert, and others. 2019. Variations in dissolved
- greenhouse gases (CO₂, CH₄, N₂O) in the Congo River network overwhelmingly driven by
- fluvial-wetland connectivity. Biogeosciences **16**: 3801–3834. doi:10.5194/bg-16-3801-2019
- Borges, A. V., F. Darchambeau, C. R. Teodoru, and others. 2015. Globally significant
- greenhouse-gas emissions from African inland waters. Nat. Geosci. 8: 637–642.
- 695 doi:10.1038/ngeo2486
- Borges, A. V, F. Darchambeau, T. Lambert, and others. 2018. Effects of agricultural land use on

- fluvial carbon dioxide, methane and nitrous oxide concentrations in a large European river,
- 698 the Meuse (Belgium). Sci. Total Environ. **610–611**: 342–355.
- 699 doi:10.1016/j.scitotenv.2017.08.047
- 700 Caruso, A., F. Boano, L. Ridolfi, D. L. Chopp, and A. Packman. 2017. Biofilm-induced
- bioclogging produces sharp interfaces in hyporheic flow, redox conditions, and microbial
- 702 community structure. Geophys. Res. Lett. **44**: 4917–4925. doi:10.1002/2017GL073651
- Clough, T. J., L. E. Buckthought, K. L. Casciotti, F. M. Kelliher, and P. K. Jones. 2011. Nitrous
- Oxide Dynamics in a Braided River System, New Zealand. J. Environ. Qual. 40: 1532–
- 705 1541. doi:10.2134/jeq2010.0527
- Cole, J. J., and N. F. Caraco. 2001. Emissions of nitrous oxide (N₂O) from a tidal, freshwater
- river, the Hudson River, New York. Environ. Sci. Technol. **35**: 991–996.
- 708 doi:10.1021/es0015848
- Covino, T., H. E. Golden, H. Y. Li, and J. Tang. 2018. Aquatic Carbon-Nutrient Dynamics as
- Emergent Properties of Hydrological, Biogeochemical, and Ecological Interactions:
- 711 Scientific Advances. Water Resour. Res. **54**: 7138–7142. doi:10.1029/2018WR023588
- 712 Crawford, J. T., R. G. Striegl, K. P. Wickland, M. M. Dornblaser, and E. H. Stanley. 2013.
- Emissions of carbon dioxide and methane from a headwater stream network of interior
- 714 Alaska. J. Geophys. Res. Biogeosciences **118**: 482–494. doi:10.1002/jgrg.20034
- 715 CSIRO. 2021. Cape Grim N2O data.
- 716 Fisher, S. G., L. J. Gray, N. B. Grimm, and D. E. Busch. 1982. Temporal Succession in a Desert
- 717 Stream Ecosystem Following Flash Flooding. Ecol. Monogr. **52**: 93–110.
- 718 doi:10.2307/2937346
- Folke, C., S. Carpenter, B. Walker, M. Scheffer, T. Elmqvist, L. Gunderson, and C. S. Holling.

- 720 2004. Regime Shifts, Resilience, and Biodiversity in Ecosystem Management. Annu. Rev.
- 721 Ecol. Evol. Syst. **35**: 557–581. doi:10.1146/annurev.ecolsys.35.021103.105711
- Gomez-Velez, J. D., J. W. Harvey, M. B. Cardenas, and B. Kiel. 2015. Denitrification in the
- 723 Mississippi River network controlled by flow through river bedforms. Nat. Geosci. 8: 941–
- 724 945. doi:10.1038/ngeo2567
- Grimm, N. B. 1987. Nitrogen Dynamics During Succession in a Desert Stream. Ecology **68**:
- 726 1157–1170. doi:1939200
- 727 Gurarie, E. 2014. bcpa.
- Gurarie, E., R. D. Andrews, and K. L. Laidre. 2009. A novel method for identifying behavioural
- 729 changes in animal movement data. Ecol. Lett. **12**: 395–408. doi:10.1111/j.1461-
- 730 0248.2009.01293.x
- Hama-Aziz, Z. Q., K. M. Hiscock, and R. J. Cooper. 2017. Indirect Nitrous Oxide Emission
- Factors for Agricultural Field Drains and Headwater Streams. Environ. Sci. Technol. 51:
- 733 301–307. doi:10.1021/acs.est.6b05094
- Holling, C. S. 1973. Resilience and Stability of Ecological Systems. Annu. Rev. Ecol. Syst. 4: 1–
- 735 23. doi:10.1146/annurev.es.04.110173.000245
- Hosen, J. D., K. S. Aho, J. H. Fair, and others. 2020. Source Switching Maintains Dissolved
- Organic Matter Chemostasis Across Discharge Levels in a Large Temperate River Network.
- 738 Ecosystems. doi:10.1007/s10021-020-00514-7
- Hu, M., D. Chen, and R. A. Dahlgren. 2016. Modeling nitrous oxide emission from rivers: a
- 740 global assessment. Glob. Chang. Biol. **22**: 3566–3582. doi:10.1111/gcb.13351
- Jencso, K. G., B. L. McGlynn, M. N. Gooseff, S. M. Wondzell, K. E. Bencala, and L. A.
- Marshall. 2009. Hydrologic connectivity between landscapes and streams: Transferring

- reach- and plot-scale understanding to the catchment scale. Water Resour. Res. **45**: 1–16.
- 744 doi:10.1029/2008WR007225
- Ladson, A. R., R. Brown, B. Neal, and R. Nathan. 2013. A standard approach to baseflow
- separation using the Lyne and Hollick filter. Aust. J. Water Resour. 17: 25–34.
- 747 doi:10.7158/W12-028.2013.17.1
- Liu, T., X. Xia, S. Liu, X. Mou, and Y. Qiu. 2013. Acceleration of Denitrification in Turbid
- Rivers Due to Denitrification Occurring on Suspended Sediment in Oxic Waters. Environ.
- 750 Sci. Technol. **47**: 4053–4061. doi:10.1021/es304504m
- Looman, A., I. R. Santos, D. R. Tait, J. R. Webb, C. A. Sullivan, and D. T. Maher. 2016. Carbon
- cycling and exports over diel and flood-recovery timescales in a subtropical rainforest
- headwater stream. Sci. Total Environ. **550**: 645–657. doi:10.1016/j.scitotenv.2016.01.082
- Maavara, T., R. Lauerwald, G. G. Laruelle, Z. Akbarzadeh, N. J. Bouskill, P. Van Cappellen, and
- P. Regnier. 2019. Nitrous oxide emissions from inland waters: Are IPCC estimates too
- 756 high? Glob. Chang. Biol. **25**: 473–488. doi:10.1111/gcb.14504
- 757 Marti, E., N. B. Grimm, and S. G. Fisher. 1997. Pre- and Post-Flood Retention Efficiency of
- Nitrogen in a Sonoran Desert Stream. J. North Am. Benthol. Soc. **16**: 805–819.
- 759 Marzadri, A., G. Amatulli, D. Tonina, A. Bellin, L. Q. Shen, G. H. Allen, and P. A. Raymond.
- 760 2021. Global riverine nitrous oxide emissions: the role of small streams and large rivers.
- 761 Sci. Total Environ. 145148. doi:10.1016/j.scitotenv.2021.145148
- Marzadri, A., M. M. Dee, D. Tonina, A. Bellin, and J. L. Tank. 2017. Role of surface and
- subsurface processes in scaling N₂O emissions along riverine networks. Proc. Natl. Acad.
- 764 Sci. **114**: 4330–4335. doi:10.1073/pnas.1617454114
- Massara, T. M., S. Malamis, A. Guisasola, J. A. Baeza, C. Noutsopoulos, and E. Katsou. 2017. A

- review on nitrous oxide (N₂O) emissions during biological nutrient removal from municipal
- wastewater and sludge reject water. Sci. Total Environ. **596–597**: 106–123.
- 768 doi:10.1016/j.scitotenv.2017.03.191
- McClain, M. E., E. W. Boyer, C. L. Dent, and others. 2003. Biogeochemical Hot Spots and Hot
- Moments at the Interface of Terrestrial and Aquatic Ecosystems. Ecosystems **6**: 301–312.
- 771 doi:10.1007/s10021-003-0161-9
- McMahon, P. B., and K. F. Dennehy. 1999. N₂O Emissions from a Nitrogen-Enriched River.
- 773 Environ. Sci. Technol. **33**: 21–25. doi:10.1021/es980645n
- Moatar, F., B. W. Abbott, C. Minaudo, F. Curie, and G. Pinay. 2017. Elemental properties,
- hydrology, and biology interact to shape concentration-discharge curves for carbon,
- 776 nutrients, sediment, and major ions. Water Resour. Res. **53**: 1270–1287.
- 777 doi:10.1002/2016WR019635
- 778 Mwanake, R. M., G. M. Gettel, K. S. Aho, D. W. Namwaya, F. O. Masese, K. Butterbach-Bahl,
- and P. A. Raymond. 2019. Land Use, Not Stream Order, Controls N₂O Concentration and
- Flux in the Upper Mara River Basin, Kenya. J. Geophys. Res. Biogeosciences **124**: 3491–
- 781 3506. doi:10.1029/2019JG005063
- National Drought Mitigation Center, U.S. Department of Agriculture, and National Ocean and
- Atmospheric Administration. 2020. National Integrated Drought Information System. U.S.
- 784 Drought Monit.
- Newcomer, M. E., S. S. Hubbard, J. H. Fleckenstein, and others. 2018. Influence of Hydrological
- Perturbations and Riverbed Sediment Characteristics on Hyporheic Zone Respiration of
- 787 CO2 and N2. J. Geophys. Res. Biogeosciences **123**: 902–922. doi:10.1002/2017JG004090
- Nielsen, L. P., P. B. Christensen, N. P. Revsbech, and J. Sørensen. 1990. Denitrification and

- oxygen respiration in biofilms studied with a microsensor for nitrous oxide and oxygen.
- 790 Microb. Ecol. **19**: 63–72. doi:10.1007/BF02015054
- O'Connor, B. L., J. W. Harvey, and L. E. McPhillips. 2012. Thresholds of flow-induced bed
- disturbances and their effects on stream metabolism in an agricultural river. Water Resour.
- 793 Res. **48**: 1–18. doi:10.1029/2011WR011488
- Outram, F. N., and K. M. Hiscock. 2012. Indirect nitrous oxide emissions from surface water
- bodies in a lowland arable catchment: A significant contribution to agricultural greenhouse
- 796 gas budgets? Environ. Sci. Technol. **46**: 8156–8163. doi:10.1021/es3012244
- Peterson, C. G., A. D. Daley, S. M. Pechauer, and others. 2011. Development of associations
- between microalgae and denitrifying bacteria in streams of contrasting anthropogenic
- 799 influence. FEMS Microbiol. Ecol. **77**: 477–492. doi:10.1111/j.1574-6941.2011.01131.x
- Pinheiro, J., D. Bates, S. DebRoy, and others. 2021. nlme: Linear and Nonlinear Mixed Effects
- 801 Models. **3.1-152**.
- Qin, X., Y. Li, S. Goldberg, and others. 2019. Assessment of Indirect N₂O Emission Factors
- from Agricultural River Networks Based on Long-Term Study at High Temporal
- Resolution. Environ. Sci. Technol. **53**: 10781–10791. doi:10.1021/acs.est.9b03896
- Qu, B., K. S. Aho, C. Li, S. Kang, M. Sillanpää, F. Yan, and P. A. Raymond. 2017. Greenhouse
- gases emissions in rivers of the Tibetan Plateau. Sci. Rep. 7. doi:10.1038/s41598-017-
- 807 16552-6
- 808 Quick, A. M., W. J. Reeder, T. B. Farrell, D. Tonina, K. P. Feris, and S. G. Benner. 2016.
- Controls on Nitrous Oxide Emissions from the Hyporheic Zones of Streams. Environ. Sci.
- 810 Technol. **50**: 11491–11500. doi:10.1021/acs.est.6b02680
- Quick, A. M., W. J. Reeder, T. B. Farrell, D. Tonina, K. P. Feris, and S. G. Benner. 2019.

812 Nitrous oxide from streams and rivers: A review of primary biogeochemical pathways and environmental variables. Earth-Science Rev. 191: 224-262. 813 814 doi:10.1016/j.earscirev.2019.02.021 815 R Core Team. 2020. R: A language and environment for statistical computing. 816 Rahm, B. G., N. B. Hill, S. B. Shaw, and S. J. Riha. 2016. Nitrate Dynamics in Two Streams 817 Impacted by Wastewater Treatment Plant Discharge: Point Sources or Sinks? J. Am. Water 818 Resour. Assoc. **52**: 592–604. doi:10.1111/1752-1688.12410 819 Ratajczak, Z., S. R. Carpenter, A. R. Ives, and others. 2018. Abrupt Change in Ecological 820 Systems: Inference and Diagnosis. Trends Ecol. Evol. 33: 513–526. 821 doi:10.1016/j.tree.2018.04.013 822 Raymond, P. A., J. E. Saiers, and W. V. Sobczak. 2016. Hydrological and biogeochemical 823 controls on watershed dissolved organic matter transport: pulse-shunt concept. Ecology 97: 824 5–16. doi:10.1890/14-1684.1 825 Reisinger, A. J., J. L. Tank, T. J. Hoellein, and R. O. Hall. 2016. Sediment, water column, and 826 open-channel denitrification in rivers measured using membrane-inlet mass spectrometry. J. 827 Geophys. Res. Biogeosciences 121: 1258–1274. doi:10.1002/2015JG003261 828 Robinson, C. T., A. R. Siebers, and J. Ortlepp. 2018. Long-term ecological responses of the 829 River Spöl to experimental floods. Freshw. Sci. 37: 433-447. doi:10.1086/699481 830 Rosamond, M. S., S. J. Thuss, and S. L. Schiff. 2012. Dependence of riverine nitrous oxide 831 emissions on dissolved oxygen levels. Nat. Geosci. 5: 715–718. doi:10.1038/ngeo1556 832 Roy Chowdhury, S., J. P. Zarnetske, M. S. Phanikumar, M. A. Briggs, F. D. Day-Lewis, and K. 833 Singha. 2020. Formation Criteria for Hyporheic Anoxic Microzones: Assessing Interactions 834 of Hydraulics, Nutrients, and Biofilms. Water Resour. Res. 56: no.

- 835 doi:10.1029/2019WR025971
- 836 Seitzinger, S. P., and C. Kroeze. 1998. Global distribution of nitrous oxide production and N
- inputs in freshwater and coastal marine ecosystems. Global Biogeochem. Cycles 12: 93–
- 838 113. doi:10.1029/97GB03657
- 839 Smith, R. L., and J. K. Böhlke. 2019. Methane and nitrous oxide temporal and spatial variability
- in two midwestern USA streams containing high nitrate concentrations. Sci. Total Environ.
- **685**: 574–588. doi:10.1016/j.scitotenv.2019.05.374
- Soued, C., P. A. Del Giorgio, and R. Maranger. 2016. Nitrous oxide sinks and emissions in
- boreal aquatic networks in Quebec. Nat. Geosci. 9: 116–120. doi:10.1038/ngeo2611
- Stanley, E. H., S. M. Powers, and N. R. Lottig. 2010. The evolving legacy of disturbance in
- stream ecology: concepts, contributions, and coming challenges. J. North Am. Benthol. Soc.
- **29**: 67–83. doi:10.1899/08-027.1
- Stow, C. A., J. T. Walker, L. Cardoch, P. Spence, and C. Geron. 2005. N2O emissions from
- streams in the Neuse River watershed, North Carolina. Environ. Sci. Technol. **39**: 6999–
- 849 7004. doi:10.1021/es0500355
- Turner, P. A., T. J. Griffis, J. M. Baker, X. Lee, J. T. Crawford, L. C. Loken, and R. T. Venterea.
- 2016. Regional-scale controls on dissolved nitrous oxide in the Upper Mississippi River.
- Geophys. Res. Lett. **43**: 4400–4407. doi:10.1002/2016GL068710
- Turnipseed, D. P., and V. B. Sauer. 2010. Discharge measurements at gaging stations, *In* U.S.
- Geological Survey Techniques and Methods book 3.
- Venkiteswaran, J. J., M. S. Rosamond, and S. L. Schiff. 2014. Nonlinear response of riverine
- N2O fluxes to oxygen and temperature. Environ. Sci. Technol. **48**: 1566–1573.
- 857 doi:10.1021/es500069j

858	Wanninkhof, R. 1992. Relationship between wind speed and gas exchange over the ocean. J.
859	Geophys. Res. 97: 7373–7382. doi:10.1029/92JC00188
860	Webb, J. R., I. R. Santos, B. Robson, B. Macdonald, L. Jeffrey, and D. T. Maher. 2017.
861	Constraining the annual groundwater contribution to the water balance of an agricultural
862	floodplain using radon: The importance of floods. Water Resour. Res. 53: 544–562.
863	doi:10.1002/2016WR019735
864	Weiss, R. F., and B. A. Price. 1980. Nitrous oxide solubility in water and seawater. Mar. Chem.
865	8: 347–359. doi:10.1016/0304-4203(80)90024-9
866	Xia, X., T. Liu, Z. Yang, G. Michalski, S. Liu, Z. Jia, and S. Zhang. 2017. Enhanced nitrogen
867	loss from rivers through coupled nitrification-denitrification caused by suspended sediment
868	Sci. Total Environ. 579 : 47–59. doi:10.1016/j.scitotenv.2016.10.181
869	Yao, Y., H. Tian, H. Shi, S. Pan, R. Xu, N. Pan, and J. G. Canadell. 2020. Increased global
870	nitrous oxide emissions from streams and rivers in the Anthropocene. Nat. Clim. Chang. 10
871	138–142. doi:10.1038/s41558-019-0665-8
872	
873	
874	
875	
876	
877	
878	
879	
880	